Research Square

Preprints are preliminary reports that have not undergone peer review.
They should not be considered conclusive, used to inform clinical practice,
or referenced by the media as validated information.

Macrophage Polarization and Osteoblast Differentiation by Photobiomodulation

Wenqi Fu
Dalian Medical University
Ok-Su Kim
Chonnam National University
Chanyong Eum
Chonnam National University
Byunggook Kim
Chonnam National University
Huiying Liu
Dalian Medical University
Guowu Ma
Dalian Medical University
Okjoon Kim
js3894@jnu.ac.kr

Chonnam National University

Research Article

Keywords: photobiomodulation, osteoimmunomodulation, osteogenesis, macrophages

Posted Date: November 10th, 2026

DOI: https://doi.org/10.21203/rs.3.rs-11338798/v1

License: This work is licensed under a Creative Commons Attribution 4.0 International License.
Read Full License

Additional Declarations: No competing interests reported.

Macrophage Polarization and Osteoblast Differentiation by Photobiomodulation

Wenqi Fu [a, b, †], Ok-Su Kim [c, e, †], Chanyong Eum [b], Byunggook Kim [d], Huiying Liu [a], Guowu Ma [a], Okjoon Kim [b, *]

a School of Stomatology, Dalian Medical University, Lvshun South Road, Dalian 116044, China
b Department of Oral Pathology, Dental Science Research Institute, School of Dentistry, Chonnam National University, Gwangju 61186, Republic of Korea
c Department of Periodontology, Dental Science Research Institute, School of Dentistry, Chonnam National University, Gwangju 61186, Republic of Korea
d Department of Oral Medicine, Dental Science Research Institute, School of Dentistry, Chonnam National University, Gwangju 61186, Republic of Korea
e Hard-Tissue Biointerface Research Center, School of Dentistry, Chonnam National University, Gwangju 61186, Republic of Korea

* Correspondence: js3894@jnu.ac.kr; Tel.: +82-62-530-4832; Fax: +82-62-530-4839
† These authors contributed equally to this work.

Abstract

Photobiomodulation therapy, represented by red light, has been established to promote tissue healing and treat bone diseases. The osteoimmune microenvironment is increasingly recognized as a critical regulator of bone regeneration, in which the transition of pro-inflammatory M1 macrophages toward a pro-regenerative M2-like phenotype plays an important role. In this study, we aimed to investigate the effects of red-light PBM on macrophage polarization and the following osteoblast differentiation. First, the M1- and M2-like macrophage polarization models were established using lipopolysaccharide (LPS) and interleukin-4 (IL-4), respectively. The pre-treatment of red light (Pre-IR+LPS) decreased the expression of M1-associated markers while increasing the expression of M2-associated markers. Morphological analysis also showed that macrophages in the Pre-IR+LPS group were elongated, resembling the M2-like macrophages. At the functional level, Pre-IR+LPS-treated macrophages showed decreased levels of LPS-induced pro-inflammatory cytokines and enhanced

osteogenic gene expression. When osteoblasts were cultured with conditioned medium derived from Pre-IR+LPS-treated macrophages, the migration and osteogenic differentiation were promoted. In contrast, Pre-IR treatment had no significant effects on IL-4-induced M2-like macrophages polarization. Taken together, these findings suggest that red light promotes the transition of M1-to-M2-like macrophage transition rather than further enhancing established M2-like polarization. Furthermore, red-light PBM creates a more osteogenesis-supportive osteoimmune microenvironment by suppressing pro-inflammatory signals and enhancing osteogenic cues in M2-like macrophages.

Keywords: photobiomodulation, osteoimmunomodulation, osteogenesis, macrophages

Introduction

Photobiomodulation (PBM) refers to the beneficial effects of regulating biological processes using red (~650 nm) or near-infrared (~750 nm) light [1]. PBM has been applied to treat bone diseases in clinical settings due to its ability to maintain homeostasis, reduce inflammation, and promote tissue healing [2]. Light in the 300-750 nm range displays a penetration depth of 0.37 to 5 mm, which is usually superficial to the bone [3]. This suggests that PBM may indirectly participate in bone healing by regulating the surrounding microenvironment. Bone regeneration is a dynamic biological process critically regulated by crosstalk between the skeletal and immune systems [4]. Light-emitting diode (LED) irradiation at 625 nm has been shown to modulate intracellular inflammatory signaling [5], suggesting its potential role in bone healing by regulating the immune microenvironment surrounding bone tissues. In this study, we aimed to explore the effects of PBM on osteogenesis through the regulation of the osteo-immune microenvironment.

Macrophages play a pivotal role in modulating the immune microenvironment by polarizing into either pro-inflammatory M1-like or pro-regenerative M2-like phenotypes [6]. Macrophages of different phenotypes not only modulate the immune

microenvironment by secreting pro- or anti-inflammatory cytokines but also regulate osteoblast differentiation by sharing common bone-related proteins. M1 macrophages enhance phagocytosis and secrete pro-inflammatory cytokines to clear pathogens and cell debris during the early stages (acute inflammatory phase) of bone healing [7]. However, the prolonged presence of M1-like macrophages can lead to chronic inflammation, which may result in delayed or impairing bone healing [8].

Following the acute inflammatory phase, M2-like macrophages create an anti-inflammatory microenvironment by releasing IL-4 and IL-10. They also secrete bone morphogenetic proteins (BMPs), osteoprotegerin (OPG), osterix (OSX), and osteocalcin (OCN), which promote osteogenesis [9,10]. In addition to these two extreme phenotypes, some macrophages show overlapping properties and are often referred to as M1-like or M2-like macrophages [9]. Given the high plasticity of macrophages and their close association with osteoblasts, appropriately regulating macrophage polarization is a rational approach to promote osteogenesis.

PBM relies on electromagnetic irradiation to induce cell-type-dependent cellular functions [11]. Macrophages are highly responsive to environmental stimuli, are found in various tissues, including bones and soft tissues [12]. PBM has been shown to modulate the activation and polarization of uncommitted macrophages toward distinct functional phenotypes [13,14]. In our previous study, we demonstrated that LED irradiation at 625 nm enhanced the mineralization of human dental pulp cells (HDPCs) through activation of mitogen-activated protein kinase (MAPK) signaling pathways [15]. However, the effects of PBM on osteogenesis through the regulation of immune microenvironment remain unclear.

To further investigate the mechanisms by which light-induced macrophage polarization promotes osteogenesis, independent datasets from the Gene Expression Omnibus (GEO) database were analyzed. Candidate genes linking inflammatory macrophage activation to impaired osteogenesis were subsequently identified through integrative analysis of publicly available transcriptomic datasets. These candidate genes were further evaluated in an independent human fracture-healing transcriptomic dataset

(GSE93387), which comprises 51 peripheral-blood gene-expression profiles obtained from fracture patients and healthy controls.

Therefore, we investigated the effects of 625-nm LED irradiation on macrophages and osteoblast differentiation. RAW264.7 cells, a monocyte/macrophage-like cell line, were irradiated, and the macrophage-conditioned medium (CM) was then used to culture MC3T3-E1 pre-osteoblasts. In parallel, transcriptomic datasets were analyzed to identify potential molecular targets linking macrophage polarization to bone healing. In the human fracture-healing dataset, expression of these genes was positively associated with M1-like macrophage signatures and inversely associated with M2-like macrophage signatures.

However, whether PBM promotes osteogenesis by reshaping macrophage-mediated osteoimmune signaling remains unclear. We therefore hypothesized that 625-nm LED irradiation promotes a shift from a pro-inflammatory macrophage state toward a pro-regenerative M2-like phenotype, thereby creating an osteoimmune microenvironment favorable for osteoblast differentiation. To test this hypothesis, we investigated the effects of 625-nm LED irradiation on macrophage polarization and evaluated the subsequent effects of macrophage-derived conditioned medium on osteoblast migration and osteogenic differentiation. In parallel, publicly available human transcriptomic datasets were analyzed to identify potential molecular signatures linking macrophage polarization to normal and impaired bone healing.

Materials and methods

Irradiation system and treatment

A 625-nm LED irradiation system was purchased from U-JIN LED (Koyang, Republic of Korea). The system was placed in a cell incubator maintained at 37 °C, 5% CO_2, and 95% relative humidity. The general procedure was identical to the previously established protocol [16,17]. The distance between the light source and the cells was set at 25 nm, and the energy delivered to the cells was set at 18 J/cm^2.

Cell culture

RAW264.7 cells were purchased from the Korean Cell Line Bank and cultured in DMEM (Gibco, Thermo Fisher Scientific, Massachusetts, USA) supplemented with 10% fetal bovine serum (FBS; Atlas Biologicals, Seoul, Republic of Korea) and 1% penicillin/streptomycin (Pen/Strep, Welgene, Gyeongsangbuk-do, Republic of Korea). The cells were passaged at around 80-90% confluence and used within 20 passages for consistent cellular properties. MC3T3-E1 pre-osteoblasts were cultured in α-MEM (Gibco, Thermo Fisher Scientific) supplemented with 10% FBS and 1% Pen/Strep. To induce differentiation, MC3T3-E1 cells were cultured in an osteogenic medium, composed of complete α-MEM, 10 mM of β-glycerophosphate, 100 nM of dexamethasone, and 50 μg/mL of ascorbic acid.

Cell viability

RAW 264.7 cells were seeded at a density of 2×10^4 cells per well in 48-well plates and cultured for 24 hours. The medium was then replaced with DMEM containing varying concentrations of LPS (0.1, 1, or 10 μg/mL) and IL-4 (20 or 40 ng/mL) with or without pre-irradiation (Pre-IR), simultaneous-irradiation (Simul-IR), or post-irradiation (Post-IR) for one hour. After an additional 24 hours, the cells were cultured in a fresh medium for 12 hours. The schematic of this experimental protocol is shown in **Fig. 1**. Subsequently, the EZ-Cytox assay kit (DoGenBio, Seoul, Republic of Korea) was used to quantify cell viability. The cells were gently washed with DPBS, followed by incubating with the EZ-Cytox working solution (1:10 dilution in FBS-free α-MEM) for 40 minutes. The optical density (OD) at 450 nm was measured using a microplate reader (BioTek, California, USA).

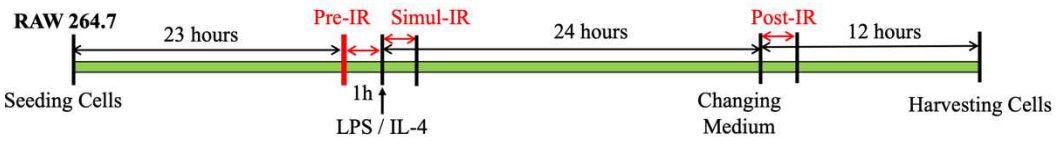


Figure 1. Schematic illustration of the macrophage treatment protocol.

ELISA

RAW 264.7 cells (2×10^4/well) were seeded in 48-well plates. The cells were treated with Pre-IR+LPS, Pre-IR+IL-4, LPS, or IL-4. The supernatant from each well was collected in 1.5 mL centrifuge tubes. The concentrations of IL-6 and TNF-α in the collected supernatant were measured using the LEGEND MAX™ ELISA Kits (Biolegend, San Diego, California, USA) for mouse IL-6 and TNF-α, respectively. The results were normalized to cell viability, which was determined using the EZ-Cytox assay.

Flow cytometry

RAW 264.7 cells were seeded in 100-mm dishes at a density of 2×10^6 cells per dish. After the treatment described above, the cells were trypsinized using TrypLE™ (Thermo Fisher Scientific, Illinois, USA), collected in 1.5-mL centrifuge tubes, centrifuged, and resuspended in PBS at a concentration of 1 x 10^6 cells/mL. The cell suspension was fixed with a fixation solution (Biolegend) for 15 minutes, followed by treatment with 0.1% Triton X-100 for 5 minutes for permeabilization. Antibodies against arginase-1 (Cell Signaling Technology, Massachusetts, USA) and iNOS (PE-conjugated; Invitrogen, Illinois, USA) were diluted 1:50 and 1:300, respectively, in PBS containing 0.5% FBS. The cells were incubated with the diluted antibodies for 30 minutes, and then with a secondary antibody (goat anti-rabbit IgG H&L-Alexa Fluor 488; Abcam, Cambridge, UK) for 15 minutes. Finally, cell sorting analysis was performed using the Accuri™ C6 Flow Cytometer (BD Biosciences, Ann Arbor, MI, USA).

Cytoskeleton staining

RAW 264.7 (1×10^5 cells per well) were seeded in cell culture slides (SPL Life Science, Gyeonggi-do, Republic of Korea). The treated cells were stained for cytoskeleton imaging using the Actin Cytoskeleton and Focal Adhesion Staining Kit (Merck KGaA, Darmstadt, Germany). The cells were first fixed with 4% paraformaldehyde (Tech&Innovation, Gangwon-do, Republic of Korea) for 5 minutes, permeabilized with

0.1% Triton X-100, and blocked with 1% bovine serum albumin (BSA) for 30 minutes. An antibody against phalloidin (TRITC-conjugated; Merck KGaA) was diluted with the blocking solution and incubated with the cells for 1 hour. Finally, the cells were incubated with DAPI for 2 minutes for nuclei staining. The slides were mounted and imaged using the Lionheart^{TM} FX system (Winooski, Vermont, USA).

RT-PCR analysis

Total RNA was isolated using the XENOPURE™ PF-Total RNA Purification Kit (XENOPURE, Gyeonggi-do, Republic of Korea) following the manufacturer's instructions and homogenized to achieve uniform concentrations. Subsequently, the cDNA was synthesized from the isolated RNA using the AccuPower® CycleScript™ RT PreMix (Bioneer, Yuseong-gu, Republic of Korea). cDNA was amplified using the primers listed in **Table 1** and the AccuPower® PCR PreMix (Bioneer). The final PCR products were subjected to gel electrophoresis using agarose gels and stained with NEOgreen (NEO science, Yuseong-gu, Republic of Korea) and visualized using the ChemiDoc XRS+ System (Bio-Rad, Massachusetts, USA).

Table 1 Primer sequences used for RT-PCR

Gene		Primer sequences (5′–3′)
BMP-2	Forward	GTGGCTGCTCAGAATTGCAG
	Reverse	CACGGCTTCTAGTTGATGGA
OCN	Forward	GCAGCTTGGTGCACACCTAG
	Reverse	ACCTTATTGCCCTCCTGCTT
RUNX2	Forward	TTTGGCTGGTTTCCCAAATA
	Reverse	TGGGGAGGATTTGTGAAGAC
OPG	Forward	AAAGCACCCTGTATAAAACA
	Reverse	CCGTTTTATCCTCTCTACACTC
COL-1	Forward	ACTCAGCCGTCTGTGCCTCA
	Reverse	GGAGGCCTCGGTGGACATTA
ALP	Forward	CCATGGTAGAATACGCTCAGAA
	Reverse	ATGGAGGATTCCAGATACAGG
OSX	Forward	CTTCCCAATCCTATTTGCCGTTT
	Reverse	CGGCCAGGTTACTAACACCAATCT
OPN	Forward	GCGTTACTGTTCAGTTTAAC

	Reverse	TGGAACTTGCTTGACTATCGA
β-actin	Forward	CCACACCTTCTACAATGAGC
	Reverse	GGCTTTCTGAACTTGACAAC

Macrophage-CM preparation

RAW 264.7 cells were treated with vehicle (Control), Pre-IR, LPS, IL-4, Pre-IR+LPS, or Pre-IR+IL-4, and the medium was replaced with fresh medium. After 24 hours of incubation, the medium from each group was collected in sterile 15 mL tubes, followed by centrifugation at 500 x *g* for 5 minutes to pellet the cells and debris. The supernatants were then transferred to new tubes. Subsequently, the RAW 264.7 culture medium was mixed with complete α-MEM at a 1:3 ratio (macrophage-CM).

Cell migration

MC3T3-E1 cells (2.5×10^5 cells/well) were seeded in 6-well plates and cultured in complete α-MEM. The cells were scratched using sterile pipette tips when the cell density reached approximately 90% confluence. Immediately after scratching, images were captured using the Lionheart^{TM} FX system in a phase-contrast channel – designated as "0 h." Subsequently, the medium was replaced with Control-CM, Pre-IR-CM, LPS-CM, IL-4-CM, Pre-IR+LPS-CM, or Pre-IR+IL-4-CM. After 20 hours of incubation, the cells were imaged again – designated as "20 h."

Alkaline phosphatase (ALP) staining and ALP activity assay

MC3T3-E1 cells were seeded in 60-mm dishes and cultured for 24 hours. The medium was then replaced with macrophage-CM with osteogenic factors and incubated for 6 days. The cells were fixed and subjected to ALP staining (Thermo Fisher Scientific) for 1 hour. The cells were scanned by a scanner (Epson, Yamagata, Japan), and detailed images were captured using the Lionheart^{TM} FX system.

Total protein was extracted to determine the ALP activity in cells. Protein concentration was measured using the BCA assay (Thermo Fisher Scientific).

Subsequently, the samples were analyzed using the SensoLyte® *p*NPP ALP assay kit (ANASPEC, California, USA). The final OD values were measured using a microplate reader and normalized based on the BCA calibration curve.

Western blot

Total proteins were extracted with RIPA buffer (Biosesang, Gyeonggi-do, Republic of Korea) containing 1% protease inhibitor cocktail (PIC; Takara, Tokyo, Japan) and 1% phenylmethanesulfonyl fluoride (PMSF; Sigma-Aldrich, Missouri, USA). The BCA assay was used to determine the protein concentrations. The samples were homogenized to a uniform level. Subsequently, the heat-inactivated samples were loaded onto SDS-PAGE gels. Electrophoresis was performed at 70 V for 1 hour, followed by 110 V for 1 hour. The separated proteins were transferred to polyvinylidene fluoride (PVDF) membranes (Cytiva, Suwon, Republic of Korea) at 90 V for 90 minutes. The membranes were blocked with 5% milk in Tris-buffered saline containing Tween-20 (TBST; MENTOS Biotechnology, Gyeongsangbuk-do, Republic of Korea) for 1 hour at room temperature. Antibodies against the following proteins were diluted in the blocking solution: iNOS, CD206, E-cadherin, Vimentin, ALP, OPN, RUNX2, β-actin, and Histone H3. The membranes were incubated with the primary antibodies overnight for 4 °C, followed by incubation with the corresponding secondary antibody for 1 hour at room temperature. Protein bands were visualized using the ChemiDoc XRS+ System, and quantitative analysis was done using the ImageJ software.

Public database analysis

All publicly available transcriptomic datasets used in this study were obtained from the Gene Expression Omnibus (GEO) database. The *in vitro* datasets included ~~the~~ GSE37558 (Late vs. Early osteogenesis) and GSE5099 (M1 vs. M0, M2 vs. M0). GSE93387, a human peripheral-blood microarray dataset of fracture healing, was used as an independent clinical validation dataset. Differential gene expression analysis of the *in vitro* datasets was performed using the limma package in R. Differentially expressed genes (DEGs) were identified using the thresholds of an absolute $\log_2$ fold

change ($|\log_2 FC|$) > 0.5 and $P < 0.05$. Using these criteria, genes significantly upregulated during osteogenic differentiation, M1-like macrophage polarization, and M2-like macrophage polarization were separately identified. Volcano plots were generated to visualize the distribution of DEGs. To identify the target gene set, an intersection analysis was conducted. Genes upregulated during osteogenic differentiation were intersected with genes upregulated in M1 macrophages, after which genes upregulated in M2 macrophages were excluded. The resulting candidate gene set was visualized using a Venn diagram. Gene Ontology (GO) biological process enrichment analysis was subsequently performed on the selected genes, and the enrichment results were visualized as bubble plots. The candidate genes were submitted to the STRING database to construct a protein–protein interaction (PPI) network. The resulting interaction network was imported into Cytoscape, and node centrality was evaluated using the maximal clique centrality (MCC) algorithm implemented in the cytoHubba plugin. The 10 genes with the highest MCC scores were designated as hub genes, and the corresponding hub gene interaction network was visualized. For validation in the GSE93387 fracture cohort, expression values for the 10 hub genes were extracted from the peripheral-blood transcriptomic dataset. Boxplots were generated using the ggpubr package, and differences in hub gene expression between the normal healing group and the nonunion group were assessed using the Wilcoxon rank-sum test. Receiver operating characteristic (ROC) curves were generated using the pROC package, and the area under the curve (AUC) was calculated for each hub gene to quantitatively evaluate its diagnostic and discriminatory performance for adverse clinical outcomes, including nonunion and delayed fracture healing. For each GSE93387 sample, the mean normalized expression of predefined M1- and M2-associated marker gene sets was calculated to derive M1- and M2-associated macrophage signature scores, respectively. Differences in M1 and M2 signature scores between the normal healing and impaired-healing samples were assessed using the Wilcoxon rank-sum test and visualized with boxplots. Finally, Spearman correlation analysis was performed to examine the associations between the expression levels of the 10 hub genes and the M1- and M2-associated macrophage signature scores.

Correlation heatmaps were generated using the pheatmap package to assess the co-expression relationships and directions of association between the in vitro-identified hub genes and macrophage polarization states (M1/M2) in the human fracture-healing dataset.

Statistical analysis

Statistical analyses were performed using ANOVA in SPSS. Statistical significance was indicated as follows: $*p < 0.05$ and $*p < 0.01$. Experiments were carried out in triplicate at a minimum to ensure reproducibility.

Results

Establishment of M1 and M2 macrophage models and their regulation by Pre-IR treatment

Macrophages were treated with varying concentrations of LPS or IL-4. As shown in **Fig. 2A**, treatment with 1 μg/mL LPS resulted in significantly higher cell viability compared to the groups treated with 0.1 and 10 μg/mL LPS. The 1 μg/mL LPS group consistently showed the highest viability among the test groups, even after Pre-IR treatment. As such, 1 μg/mL LPS was selected as the optimal concentration for subsequent experiments. For IL-4, 20 ng/mL was chosen as the optimal concentration, as 40 ng/mL led to a reduction in cell viability.

Western blot analyses of cells treated with LPS and IL-4 are shown in **Fig. 2B**. LPS at 1 μg/mL was found to induce M1 marker (iNOS) expression while IL-4 at 20 ng/mL stimulated M2 marker (CD206) expression. These results confirmed the ability of the respective concentrations to mediate macrophage polarization into M1 and M2 models. Importantly, Pre-IR treatment (Pre-IR+LPS and Pre-IR+IL-4) significantly decreased iNOS expression in M1 macrophages while increasing CD206 expression in M2 macrophages. However, irradiation alone did not alter the expression of either protein.

As shown in **Fig. 2C**, flow cytometry further revealed the effects of Pre-IR on macrophage polarization. Compared to the Control group, the LPS-treated group showed a shift in the cell population to the lower-right quadrant – 47.90 ± 4.34% of the

population showed high iNOS/low Arginase ($iNOS^+/Arginase^-$) expression, confirming their polarization into the M1 phenotype. Only 30.27 ± 5.42% of the Pre-IR+LPS cell population showed $iNOS^+/Arginase^-$ expression, indicating that Pre-IR inhibited M1 polarization. In addition, the respective cell population showed a shift towards the upper-right quadrant ($iNOS^+/Arginase^+$), increasing from 32.57 ± 2.16% to 49.30 ± 2.46% compared to the LPS-treated group. These results suggest that macrophages

exhibited a tendency to polarize M1-like macrophages to an M2-like phenotype following irradiation.

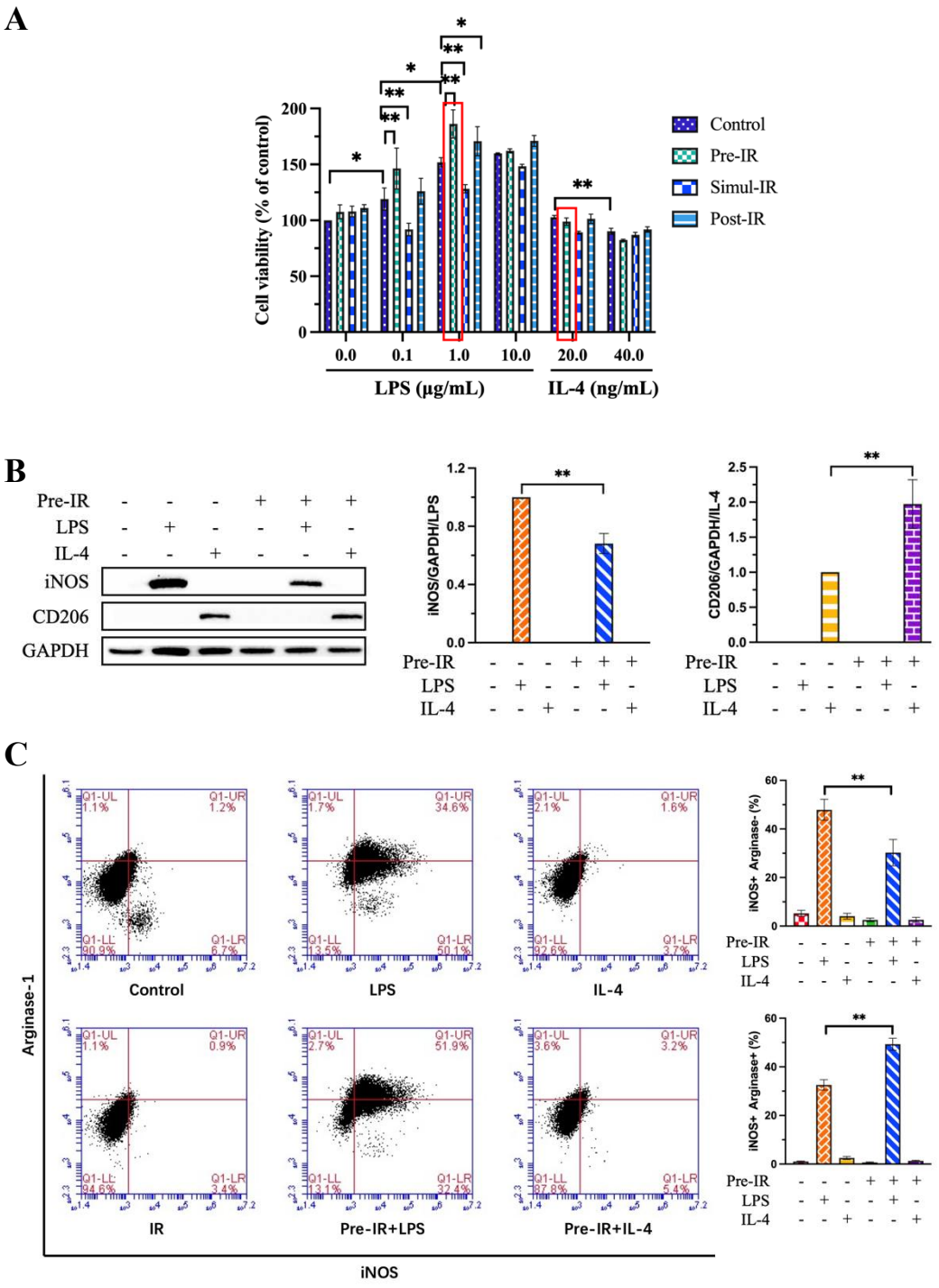


Figure 2. Establishment of M1 and M2 macrophage models and their regulation using Pre-IR. (A) RAW 264.7 cell viability after treatment with varying concentrations of LPS or IL-4 for 24 hours, with or without Pre-IR, Simul-IR, or Post-IR. (B) Expression of iNOS and CD206, macrophage phenotypic markers, were determined by western

blot analysis. (C) The of macrophage phenotype was analyzed by flow cytometry. The percentages of $iNOS^+/Arginase^-$ and $iNOS^+/Arginase^+$ cell populations were quantified and showed as mean ± standard error of the mean (SEM) in the histograms.

Pre-IR induced M2-like macrophage morphology

Cytoskeleton staining was performed to observe macrophage morphology, as shown in **Fig. 3**. The Control group (naïve M0 macrophages) appeared round and lacked pseudopods. LPS treatment induced the formation of filopodia and a significant increase in the cell spreading area, as revealed by quantitative analysis. Conversely, IL-4 treatment led to cell elongation and caused a polar distribution of actin. Immunofluorescence staining further showed that IL-4-treated macrophages were significantly elongated, exhibiting a spindle-like shape, with actin accumulating at the cell poles (marked with green asterisks). The elongation ratio was found to be the highest in the IL-4-treated group among the test groups. Additionally, although Pre-IR-activated macrophages were not as significantly polarized as those in the IL-4 group, they still exhibited an elongated, M2-like morphology. Interestingly, both Pre-IR+LPS and Pre-IR+IL-4 groups developed lamellipodia-like structures (marked with red asterisks), which were not observed in any other groups.

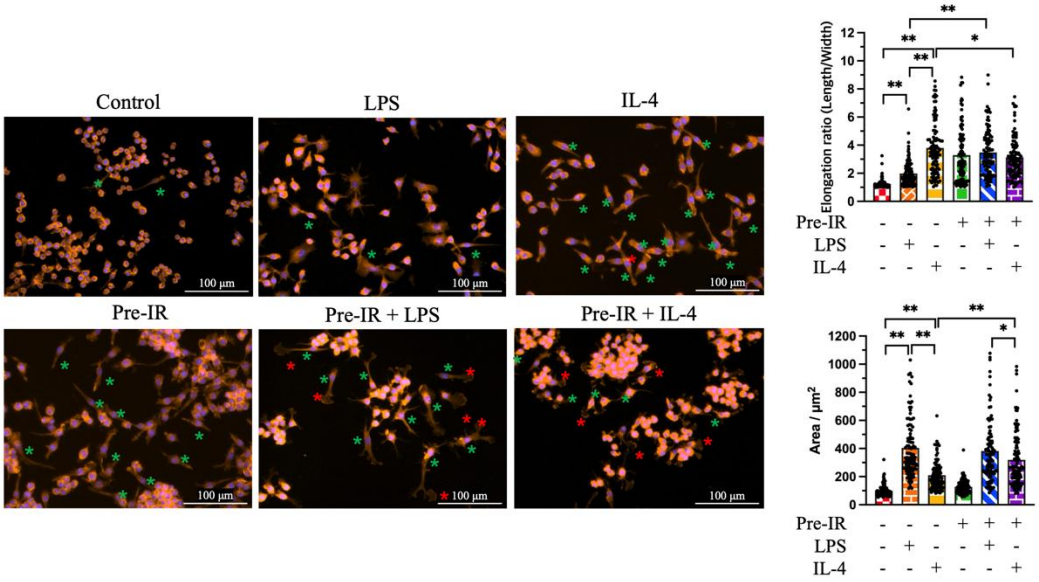


Figure 3. Pre-IR-induced changes in macrophage morphology. The analysis was conducted on cells stained with TRITC-conjugated phalloidin (red) for actin skeleton

and DAPI (blue) for nuclei. The cellular spreading areas and elongation factors (the ratio of the long axis to the short axis) were quantified for further analysis. Scale bars: 100 μm. Green asterisk: elongated cells. Red asterisk: lamellipodia-like structure.

Pre-IR mitigated pro-inflammatory cytokine release and promoted osteogenic gene expression in macrophages

The levels of macrophage-released pro-inflammatory cytokines are shown in **Fig. 4A**. Compared to LPS treatment alone, Pre-IR+LPS significantly reduced TNF-α and IL-6 concentrations in the cell supernatant. IL-4, Pre-IR, and Pre-IR+IL-4 exhibited cytokine levels similar to those of the Control group. **Fig. 4B** shows the osteogenic gene expression levels in macrophages. The Control group exhibited basal levels of osteogenic genes. Compared to this baseline, LPS treatment reduced BMP-2, OCN, RUNX2, OPG, and ALP expression, whereas Pre-IR+LPS restored their levels. In particular, COL-1 and OSX expression was increased in the respective group. Compared to the Control group, IL-4 treatment upregulated BMP-2, OCN, RUNX2, COL-1, and OSX expression. Among these genes, BMP-2 and RUNX2 expression were further enhanced while OSX and OPG levels were reduced by Pre-IR+IL-4 treatment.

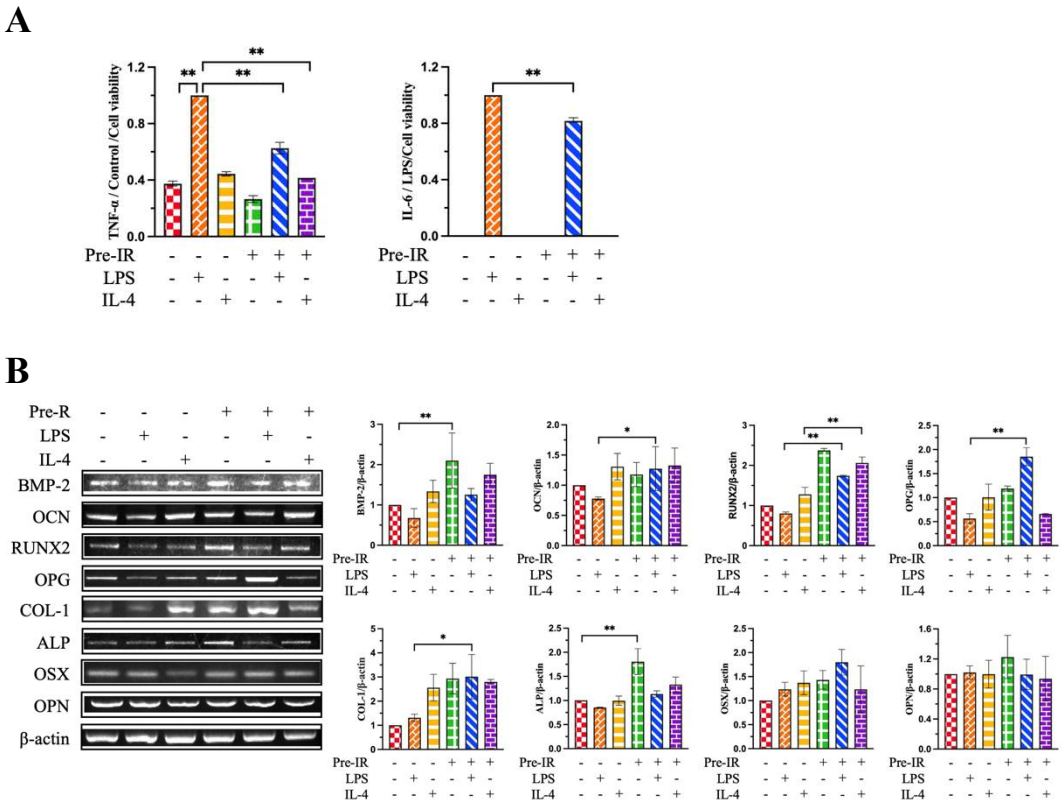


Figure 4. Pre-IR mitigated pro-inflammatory cytokine release and promoted osteogenic gene expression in macrophages. (A) Pre-IR reduced TNF-α and IL-6 secretion induced by LPS treatment. (B) Osteogenic genes, including BMP-2, OCN, RUNX2, OPG, COL-1, ALP, OSX, and OPN, were modulated by Pre-IR treatment in macrophages.

Pre-IR-treated macrophage-CM promoted MC3T3-E1 cell migration and the corresponding protein expression

The effects of macrophage-CM on MC3T3-E1 cell migration are shown in **Fig. 5**. The experimental timeline is depicted in **Fig. 5A**. The cell scratch assay (**Fig. 5B**) demonstrated that LPS-CM inhibited cell migration. However, this inhibitory effect was mitigated by Pre-IR (Pre-IR+LPS-CM). In contrast, IL-4-CM promoted cell migration, which was further accelerated by Pre-IR (Pre-IR+IL-4-CM).

The expression levels of migration-related proteins, E-cadherin and vimentin, are shown in **Fig. 5C**. The Pre-IR+LPS-CM group showed a reduced level of LPS-induced E-cadherin expression. Other than the LPS-CM group, there was no significant difference in E-cadherin levels between the treated groups and the Control-CM group.

In contrast, compared to the LPS-CM group, the Pre-IR+LPS-CM group showed increased vimentin expression. Furthermore, the Pre-IR+IL-4-CM group enhanced the effects of IL-4-CM on promoting vimentin expression.

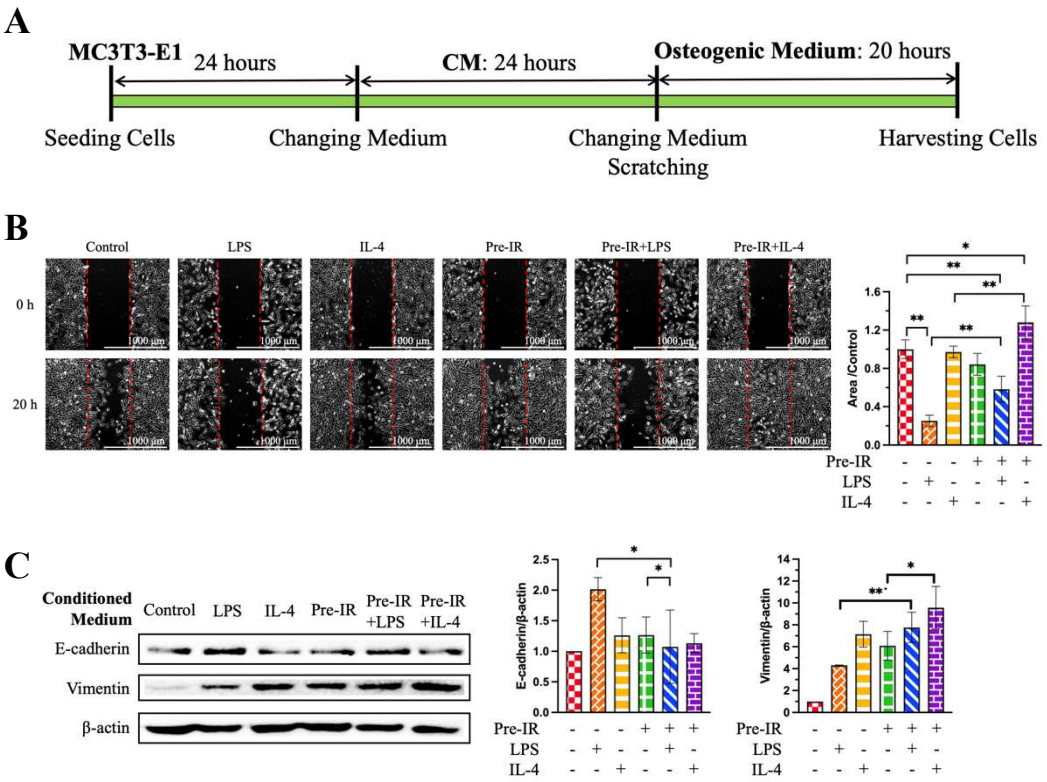


Figure 5. Pre-IR-treated macrophage-CM promoted MC3T3-E1 migration and its related proteins. (A) Experimental protocol for treating MC3T3-E1 with macrophage-CM to assess its impact on cell migration. (B) The migration of MC3T3-E1 was enhanced by culturing in Pre-IR-treated macrophage CM. (C) The expression of migration-related proteins in MC3T3-E1 cells was regulated by Pre-IR-treated macrophage-CM. Scale bars: 1000 μm

Pre-IR-treated macrophage-CM promoted osteogenic differentiation of MC3T3-E1 cells

MC3T3-E1 cells were treated following the experimental schedule shown in **Fig. 6A**. ALP staining (**Fig. 6B**) demonstrated that the LPS-CM group showed a reduced level of purple precipitation compared to the Control-CM group. In contrast, the IL-4-CM and Pre-IR-CM groups showed increased deposition of purple precipitates. Moreover, the Pre-IR+LPS-CM group showed a higher level of staining than the LPS-CM group,

while the Pre-IR+IL-4-CM group showed further enhanced deposition of purple precipitates. Quantified ALP activity showed a similar trend (**Fig. 6C**). However, the difference between IL-4-CM and Pre-IR+IL-4-CM groups was not statistically significant.

The expression of osteogenesis-related proteins and transcription factors is shown in **Fig. 6D**. The Pre-IR+LPS-CM group showed enhanced levels of ALP and OPN proteins compared to the LPS-CM group. However, RUNX2 expression in nuclei was found to be lower in the Pre-IR+LPS-CM group. Additionally, the IL-4-CM group showed increased levels of ALP, OPN, and RUNX2 expression, whereas the Pre-IR+IL-4-CM group showed decreased expression of these markers. However, RUNX2 expression in nuclei was lower in Pre-IR+LPS-CM group. Additionally, IL-4-CM increased ALP, OPN, and RUNX2 expression, whereas Pre-IR+IL-4-CM decreased their expression.

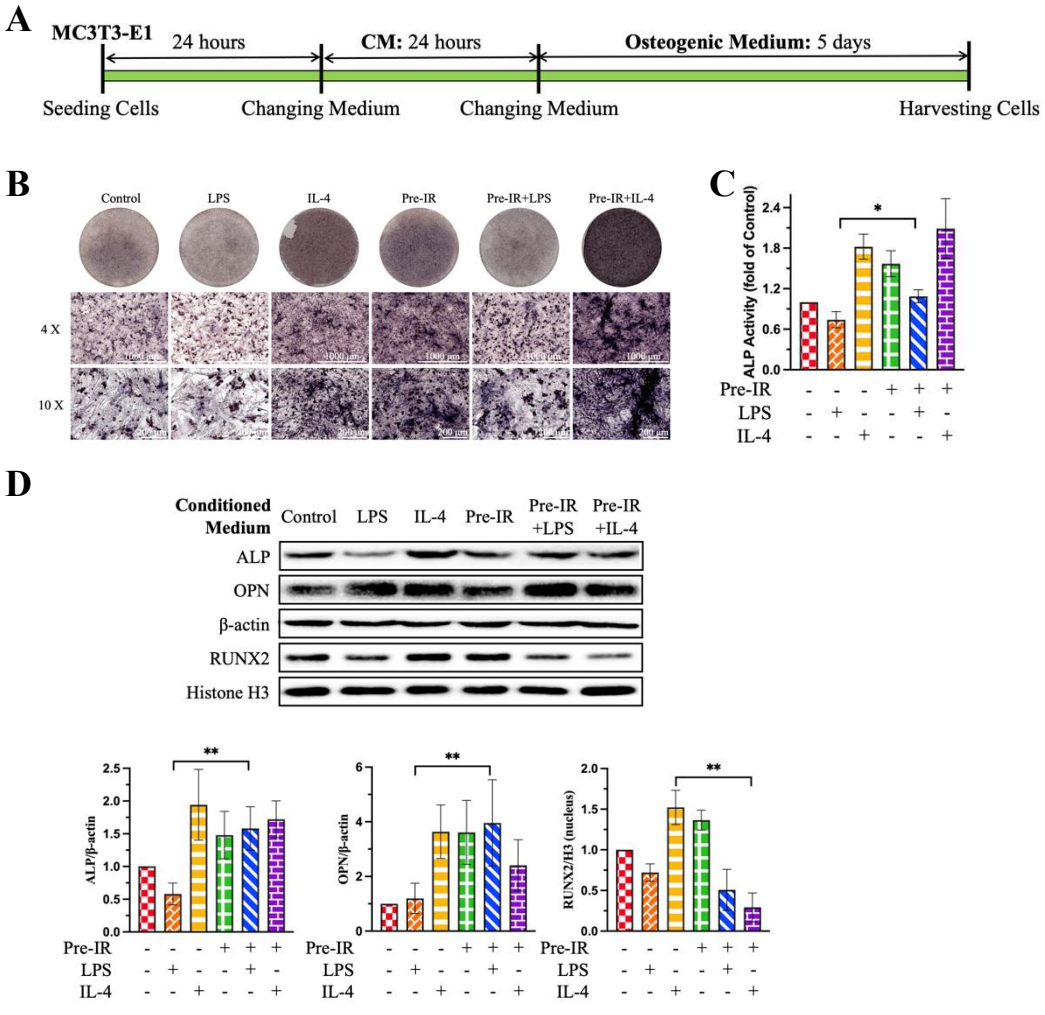


Figure 6. Pre-IR-treated macrophage-CM promotes osteogenic differentiation of MC3T3-E1 cells. (A) The experimental protocol for treating MC3T3-E1 cells with macrophage-CM to assess the impact on osteogenic differentiation. (B) MC3T3-E1 cells exhibited increased ALP deposition when cultured in Pre-IR-treated macrophage-CM. (C) Pre-IR-treated macrophage-CM enhanced the ALP activity of MC3T3-E1 cells. (D) Pre-IR-treated macrophage-CM regulated the expression of osteogenic proteins in MC3T3-E1 cells. Scale bars: 1,000 μm at 4x magnification; 200 μm at 10x magnification.

Identification of M1 macrophage-associated gene signatures linked to osteogenesis

Differential gene expression patterns the GSE37558 and GSE5099 datasets are presented in **Fig. 7**. The volcano plots in **Fig. 7A** revealed numerous differentially expressed genes between the early and late stages of osteogenesis. As shown in **Fig. 7B** and **7C**, both M1- and M2- polarized macrophages exhibited distinct transcriptional changes compared with M0 macrophages. To identify the key gene set associated with osteogenesis-related M1 macrophages, a multiple-set intersection analysis was performed. As shown in the Venn diagram in **Fig. 7D**, 84 genes were shared between the osteogenesis-upregulated and M1-upregulated gene sets. After excluding seven genes that were also upregulated in M2 macrophages, 77 M1-associated candidate genes remained.

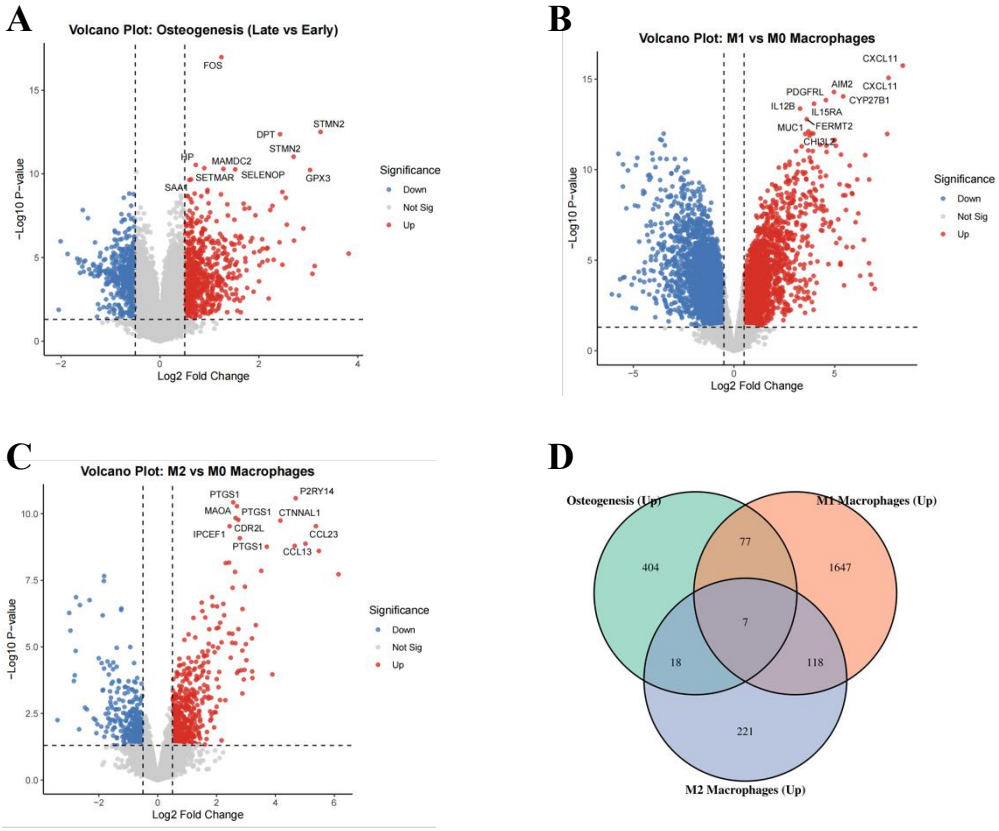


Figure 7. Identification of key gene signatures underlying M1 macrophage-driven osteogenesis. (A) Volcano plot of differentially expressed genes in Late vs. Early osteogenesis. (B, C) Volcano plots of differentially expressed genes for M1 vs. M0 and M2 vs. M0 macrophages. (D) Venn diagram illustrating the intersecting genes among the osteogenesis, M1 macrophage, and M2 macrophage gene sets.

Construction and enrichment analysis of the candidate gene networks

A protein–protein interaction (PPI) network was constructed for the 77 candidate genes using the STRING database to assess their network connectivity. Topological analysis using the maximal clique centrality (MCC) algorithm identified the top 10 hub genes with the highest MCC scores: IFIT2, IFITM1, IFITM3, MX1, OAS2, IFI44L, TRIM22, GBP2, IFITM2, and CCL5 (**Fig. 8A**). These genes formed a highly interconnected module within the PPI network, suggesting coordinated involvement in M1-associated inflammatory and osteogenic processes.

Functional enrichment analysis of the 77 candidate genes is presented in the bubble plot in **Fig. 8B**. These genes were enriched in biological processes related to response to virus, leukocyte cell–cell adhesion, regulation of fat cell differentiation, and response to type II interferon.

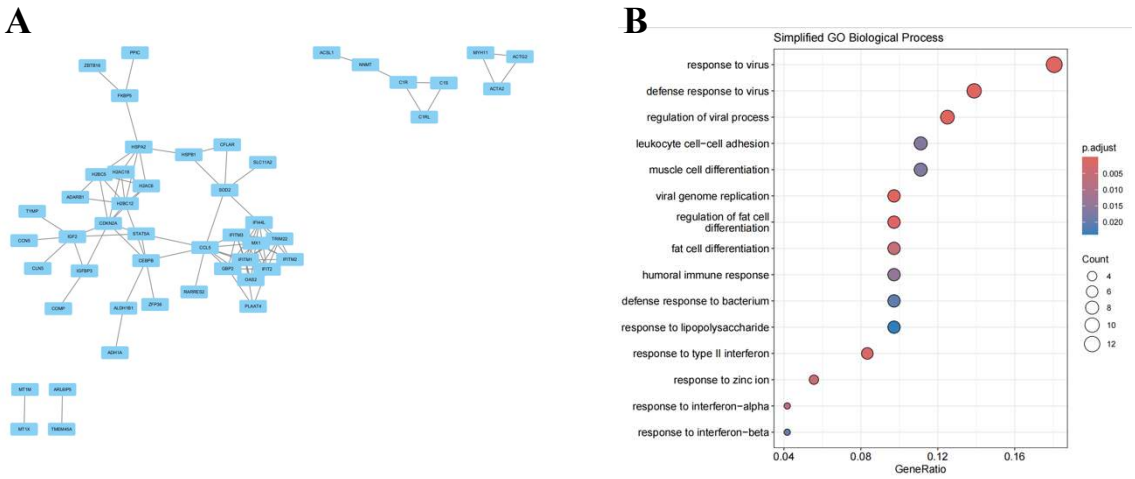


Figure 8. Construction and functional enrichment analysis of candidate gene networks. (A) Protein–protein interaction network of the top 10 hub genes. (B) Bubble plot of functional enrichment analysis for the 77 candidate genes.

Validation of hub genes in a human fracture-healing microarray dataset

The 10 hub genes were further evaluated in the GSE93387 human peripheral-blood microarray dataset of fracture healing, comprising 51 expression profiles. The 10 hub genes identified from the intersection of osteogenesis- and M1-associated transcriptional signatures were evaluated in this dataset. The dataset included samples from normal and impaired fracture-healing outcomes, allowing the clinical relevance of the hub genes to be evaluated in the context of fracture healing.

As shown in **Fig. 9A**, seven of the 10 hub genes—IFIT2, IFITM1, MX1, OAS2, IFI44L, TRIM22, and GBP2—were significantly upregulated in the impaired-healing group compared with the normal-healing group ($P < 0.05$). The area under the curve (AUC)

values indicated that several individual genes exhibited potential diagnostic utility (**Fig. 9B**). Among these genes, IFI44L showed the highest AUC (0.79), followed by MX1 (0.78), GBP2 (0.77), and IFITM1 (0.74). M1- and M2-associated macrophage transcriptional signature scores were further compared between the normal- and impaired-healing groups (**Fig. 9C**). No statistically significant differences were observed between the Normal and Disease groups in either M1 macrophage signature scores (P = 0.23) or M2 macrophage signature scores (P = 0.76). In **Fig. 9D**, Spearman correlation analyses were performed between the expression levels of the 10 hub genes and the signature scores of M1 and M2 macrophages. The correlation heatmap revealed distinct patterns of association with the M1- and M2-associated signatures. Several hub genes, including OAS2, MX1, IFITM3, and TRIM22, were positively correlated with M1 macrophage infiltration scores. In contrast, these genes tended to show inverse correlations with M2 macrophage signature scores. For example, the Spearman correlation coefficients with M2 macrophage signature were -0.38 for OAS2, -0.33 for MX1, and -0.31 for IFI44L.

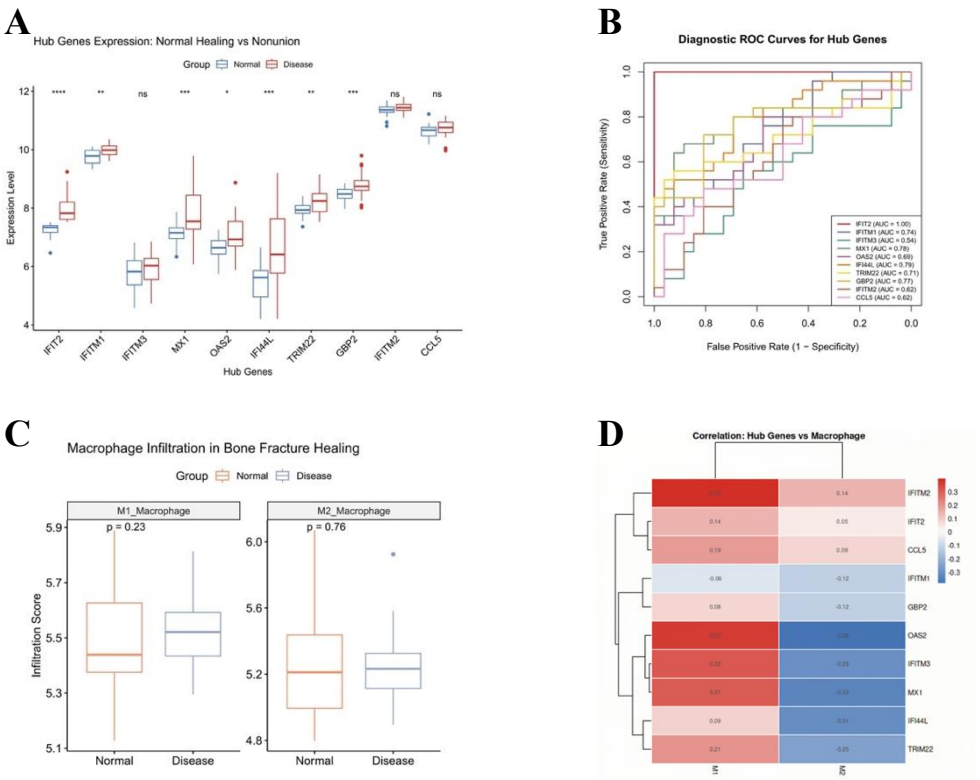


Figure 9. Validation of hub genes in a human peripheral-blood fracture healing. (A) Comparision of the expression levels of 10 hub genes between Normal- and impaired-healing groups. (B) Receiver operating characteristic (ROC) curve analysis was performed to evaluate the ability of individual hub genes to discriminate between normal fracture healing and nonunion. (C) Comparison of M1- and M2-associated macrophage signature scores derived from predefined marker gene sets in normal- and impaired-healing samples. (D) Clustered heatmap of Spearman correlations between hub gene expression and M1- and M2-associated macrophage signature scores.

Discussion

PBM is a noninvasive therapeutic modality used clinically for pain relief, modulation of inflammation, and tissue repair [15,18–20]. However, the underlying mechanisms that contribute to these effects remain poorly understood. Recent studies have demonstrated that red light modulate macrophage polarization, a process that play an important role in immunomodulation and bone regeneration. Our previous study revealed that red light can regulate intracellular protein homeostasis, thereby directly promoting osteogenic differentiation in osteoblasts. Given the close crosstalk between the skeletal and immune systems, we further investigated whether red-light PBM influences osteogenesis through macrophage-mediated osteoimmune regulation.

Bone healing usually comprises three overlapping phases: inflammation, bone formation, and remodeling [21]. Macrophages, characterized by high plasticity, are involved in all three processes. They are among the first immune cells to respond to the injury, facilitating debris clearance, phagocytosis of dead cells and pathogens and pro-inflammatory cytokine release [22]. Following the initial inflammatory response, macrophages transition from a pro-inflammatory phenotype (M1) to a regenerative phenotype (M2), a critical shift from inflammation to tissue repair [23,24]. To model inflammatory and pro-regenerative macrophage polarization in vitro, RAW264.7 cells were treated with LPS and IL-4 to induce M1- and M2-like states, respectively (**Fig. 2A** and **B**). The effects of Pre-IR on macrophage phenotype and function were subsequently examined.

As shown in **Fig. 2B and C**, Pre-IR reduced M1 marker expression while enhancing M2 marker expression in LPS-stimulated macrophages. However, irradiation alone did not significantly alter canonical M1- or M2-associated markers, indicating that PBM alone was insufficient to induce overt macrophage polarization under basal conditions. This activation can influence the subsequent polarization [25]. Cell morphology, a known indicator of macrophage polarization, is highly sensitive to environmental changes [22,26]. Therefore, cellular morphology was further examined as an additional indicator of macrophage phenotype. **Fig. 3** demonstrated that Pre-IR treatment altered cell morphology, inducing an elongated shape characteristic of M2-like macrophages [26,27]. Moreover, Pre-IR upregulated osteogenesis-related genes, including BMP-2, RUNX2, COL-1, and ALP, while having no impact on TNF-α and IL-6 expression (**Fig. 4B**). Previous studies have shown that activated macrophages show distinct gene expression profiles unrelated to cytokine release [25]. Our previous study also demonstrated that red light treatment enhances the expression of chaperone protein, providing protective effects in a highly stimulated environment [17]. Thus, these findings suggest that Pre-IR indeed activates macrophages to prepare them for subsequent stimuli.

To investigate the role of red light in macrophage phenotype transition, flow cytometry was performed (**Fig. 2C**). Under inflammatory condition, Pre-IR increased the proportion of $iNOS^+/Arginase^+$ double-positive macrophages, consistent with a intermediate phenotype between the M1 and M2 forms. As shown in **Fig. 3**, the Pre-IR+LPS macrophages exhibited increased cell elongation characteristic of M2 macrophages [26,27]. Morphologically, lamellipodia-like protrusions (marked with red asterisks) were observed predominantly in Pre-IR+LPS- and Pre-IR+IL-4-treated macrophages (Fig. 3). These cytoskeletal actin protrusions play a role in driving cell migration [28,29]. From a physiological perspective, M1 macrophages remain at the infected site to clear pathogens, while M2 macrophages migrate to facilitate tissue repair [30,31]. These morphological changes suggest that irradiation may alter cytoskeletal organization and migratory potential; however, direct macrophage

migration assays would be required to confirm this interpretation. The Pre-IR+LPS group showed a reduced level of pro-inflammatory cytokine release while upregulating osteogenic gene expression (**Fig. 4**). These findings demonstrated that the Pre-IR+LPS macrophages functioned similarly to M2-like macrophages, which promote tissue repair [32]. However, there was no significant difference between the IL-4 and Pre-IR+IL-4 groups. As M1 and M2 phenotypes represent the two extremes of the complex macrophage phenotype spectrum [33,34], recent studies have proposed the concept of M1-like and M2-like macrophages [7,35,36]. Thus, Pre-IR appeared to preferentially redirect LPS-induced inflammatory macrophages toward an M2-like phenotype rather than further enhancing IL-4-induced M2-like polarization.

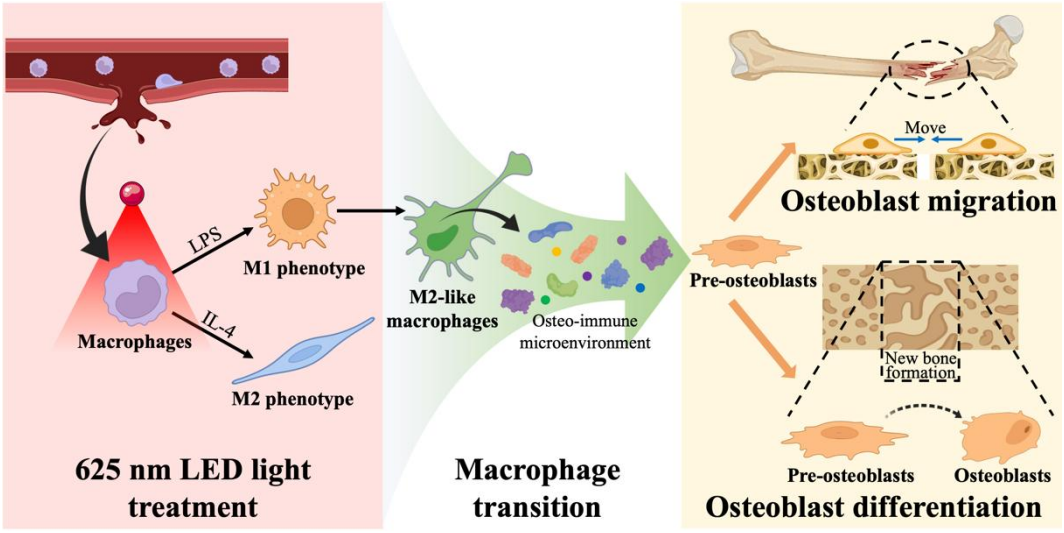
Macrophages participate in bone regeneration through cytokine secretion and osteogenic signaling [10]. As shown in **Fig. 4A**, the Pre-IR+LPS group showed a reduced level of LPS-induced pro-inflammatory cytokine release. These findings suggest that Pre-IR attenuated excessive inflammatory signaling and contributed to a microenvironment more favorable for osteogenesis. Analysis of osteogenesis-related transcripts in macrophages (Fig. 4B) revealed differential regulation of genes classically associated with osteoblast differentiation and mineralization [37,38]. Compared to LPS alone, Pre-IR+LPS increased the expression of RUNX2, COL-1, and ALP genes, which facilitate the maturation of pre-osteoblasts [39]. The increased levels of OCN and OPG contribute to the mineralization phase [40,41]. However, with the exception of RUNX2, no significant differences in osteogenesis-related gene expression were observed between the IL-4 and Pre-IR+IL-4 groups, consistent with the flow-cytometric findings.

To confirm the osteogenic functions of Pre-IR treated macrophages, CM was used to transfer macrophage-derived biological cues to osteoblasts. A wound-healing assay was performed to assess osteoblast migratory capacity. As shown in **Fig. 5B**, Pre-IR+LPS-CM restored LPS-induced cell migration inhibition, while Pre-IR+IL-4-CM increased cell migration beyond the effects induced by IL-4-CM. To elucidate the underlying mechanism, the expression of E-cadherin and vimentin – cell migration-related proteins – was analyzed. E-cadherin, a cell-cell adhesion molecule, disrupts

migration, whereas vimentin promotes migration by modulating cytoskeletal dynamics [42-45]. **Fig. 5C** showed that Pre-IR+LPS-CM decreased E-cadherin expression while increasing vimentin expression, consistent with its relevance to cell migration and protein expression. Similarly, Pre-IR+LPS-CM enhanced ALP staining and activity, along with the expression of associated proteins (ALP and OPN) (**Fig. 6**). However, there was no significant difference between the IL-4-CM and Pre-IR+IL-4-CM groups. Previous studies have demonstrated that alleviating inflammation is beneficial to bone regeneration, and even low levels of inflammatory cytokines can promote osteogenesis [46-48]. Additionally, M2 or M2-like macrophages have been demonstrated to support osteoblast migration and differentiation by secreting osteogenic factors [35,49,50].

Based on the above cellular experimental results, osteogenesis-related genes in M1 macrophages were further screened and analyzed. Bioinformatics analyses were performed using the GSE37558, GSE5099, and GSE93387 datasets. Integrated analysis of the in vitro transcriptomic datasets identified 10 network-central hub genes shared between M1-associated and osteogenesis-related transcriptional signatures (**Figs. 7 and 8**). A characteristic pathological feature of nonunion is the prolongation of inflammation, with retention of the immune microenvironment in an M1-dominant pro-inflammatory state [51]. The expression patterns of the 10 hub genes were subsequently evaluated in the human peripheral-blood fracture-healing dataset GSE93387. Several hub genes were significantly upregulated in impaired-healing samples, consistent with persistence of an inflammation-associated transcriptional program during unsuccessful fracture healing (**Fig. 9A**). The finding in **Fig. 9B** suggest that altered expression of these genes may serve as potential early molecular indicators for impaired fracture healing and the risk of nonunion. As shown in **Fig. 9C**, no significant differences were detected between the normal- and impaired-healing groups in either the M1- or M2-associated macrophage signature scores. These findings suggest that differences in individual inflammation-related genes may occur even in the absence of detectable group-level differences in the composite M1- and M2-associated transcriptional scores. These correlation patterns in the clinical cohort were consistent with the screening rationale derived from the initial datasets, GSE37558 and GSE5099 (**Fig. 9D**). The

identified genes may therefore represent an inflammation-associated gene module that is positively related to M1-like transcriptional signatures and inversely related to M2-like signatures. Analysis of the independent human fracture-healing dataset provided preliminary translational support for the clinical relevance of several hub genes identified from the in vitro datasets. Among the hub genes, IFI44L, MX1, and GBP2 emerged as candidate molecular signatures associated with persistent inflammatory macrophage states and impaired fracture healing. Their positive associations with M1-like transcriptional signatures and inverse associations with M2-like signatures suggest that suppression of this inflammatory gene module may accompany the macrophage reprogramming induced by PBM. Nevertheless, the present bioinformatic analysis does not establish these genes as direct molecular targets of Pre-IR, and further experimental studies are required to determine whether PBM directly regulates their expression and whether such regulation contributes to the transition toward an M2-like, osteogenesis-supportive macrophage phenotype. Followed by optimizing the osteo-immune microenvironment by regulating M2-like macrophage polarization, thereby reducing pro-inflammatory cytokines and regenerating osteogenic cues to promote bone regeneration. Collectively, these findings support a model in which Pre-IR attenuates LPS-driven inflammatory signaling, promotes the acquisition of M2-like macrophage features, and enhances macrophage-derived cues that favor osteoblast migration and osteogenic differentiation.



Scheme illustration of the osteoimmunomodulation effects of 625 nm LED irradiation. Pre-treatment with red light (Pre-IR+LPS) shifted LPS-stimulated macrophages toward an M2-like phenotype rather than further enhancing IL-4-induced M2-like polarization. This phenotypic and functional reprogramming attenuated pro-inflammatory signaling and enhanced macrophage-derived pro-osteogenic cues, thereby creating an osteoimmune microenvironment favorable for osteoblast migration and osteogenic differentiation.

CRediT authorship contribution statement

Wenqi Fu: Writing – original draft, Writing – review and editing, Investigation. **Ok-Su Kim:** Writing – review and editing, Visualization. **Chanyong Eum:** Software. **Byunggook Kim:** Investigation, Methodology. **Huiying Liu:** Project administration. **Guowu Ma:** Supervision. **Okjoon Kim**: Writing – review and editing, Supervision.

Declaration of Competing Interest

The authors declare that they have no known competing financial interests or personal relationships that could have appeared to influence the work reported in this paper.

Funding

This work was supported by the National Research Foundation of Korea(NRF) grant funded by the Korea government(MSIT) (No. RS-2026-25478544, RS-2026-25475340) and the Youth Talent Cultivation Fund Project of Dalian Medical University (xqnky202518).

References:

1. Clement, M.; Daniel, G.; Trelles, M. Optimising the design of a broad-band light source for the treatment of skin. *J Cosmet Laser Ther* **2005**, *7*, 177-189, doi:10.1080/14764170500344575.
2. Dompe, C.; Moncrieff, L.; Matys, J.; Grzech-Lesniak, K.; Kocherova, I.; Bryja, A.; Bruska, M.; Dominiak, M.; Mozdziak, P.; Skiba, T.H.I.; et al. Photobiomodulation-Underlying Mechanism and Clinical Applications. *J Clin Med* **2020**, *9*, doi:10.3390/jcm9061724.
3. Ash, C.; Dubec, M.; Donne, K.; Bashford, T. Effect of wavelength and beam width on penetration in light-tissue interaction using computational methods. *Lasers Med Sci* **2017**, *32*, 1909-1918, doi:10.1007/s10103-017-2317-4.
4. Lee, S.H.; Choi, Y. Communication between the skeletal and immune systems. *Osteoporosis and Sarcopenia* **2015**, *1*, 81-91, doi:10.1016/j.afos.2015.09.004.
5. Sun, Q.; Kim, H.E.; Cho, H.; Shi, S.; Kim, B.; Kim, O. Red light-emitting diode irradiation regulates oxidative stress and inflammation through SPHK1/NF-kappaB activation in human keratinocytes. *J Photochem Photobiol B* **2018**, *186*, 31-40, doi:10.1016/j.jphotobiol.2018.05.015.
6. Pajarinen, J.; Lin, T.; Gibon, E.; Kohno, Y.; Maruyama, M.; Nathan, K.; Lu, L.; Yao, Z.; Goodman, S.B. Mesenchymal stem cell-macrophage crosstalk and bone healing. *Biomaterials* **2019**, *196*, 80-89, doi:10.1016/j.biomaterials.2017.12.025.
7. Kohno, K.; Koya-Miyata, S.; Harashima, A.; Tsukuda, T.; Katakami, M.; Ariyasu, T.; Ushio, S.; Iwaki, K. Inflammatory M1-like macrophages polarized by NK-4 undergo enhanced phenotypic switching to an anti-inflammatory M2-like phenotype upon co-culture with apoptotic cells. *J Inflamm (Lond)* **2021**, *18*, 2, doi:10.1186/s12950-020-00267-z.
8. Sridharan, R.; Cameron, A.R.; Kelly, D.J.; Kearney, C.J.; O'Brien, F.J. Biomaterial based modulation of macrophage polarization: a review and suggested design principles. *Materials Today* **2015**, *18*, 313-325, doi:10.1016/j.mattod.2015.01.019.
9. Strizova, Z.; Benesova, I.; Bartolini, R.; Novysedlak, R.; Cecrdlova, E.; Foley, L.K.; Striz, I. M1/M2 macrophages and their overlaps - myth or reality? *Clin Sci (Lond)* **2023**, *137*, 1067-1093, doi:10.1042/CS20220531.
10. Chen, Z.; Bachhuka, A.; Wei, F.; Wang, X.; Liu, G.; Vasilev, K.; Xiao, Y. Nanotopography-based strategy for the precise manipulation of osteoimmunomodulation in bone regeneration. *Nanoscale* **2017**, *9*, 18129-18152, doi:10.1039/c7nr05913b.
11. Felician, M.C.P.; Belotto, R.; Tardivo, J.P.; Baptista, M.S.; Martins, W.K. Photobiomodulation: Cellular, molecular, and clinical aspects. *Journal of Photochemistry and Photobiology* **2023**, *17*, doi:10.1016/j.jpap.2023.100197.
12. Sinder, B.P.; Pettit, A.R.; McCauley, L.K. Macrophages: Their Emerging Roles in Bone. *J Bone Miner Res* **2015**, *30*, 2140-2149, doi:10.1002/jbmr.2735.
13. Tian, T.; Wang, Z.; Chen, L.; Xu, W.; Wu, B. Photobiomodulation activates undifferentiated macrophages and promotes M1/M2 macrophage

polarization via PI3K/AKT/mTOR signaling pathway. *Lasers Med Sci* **2023**, *38*, 86, doi:10.1007/s10103-023-03753-x.
14. Liao, W.T.; Hung, C.H.; Liang, S.S.; Yu, S.; Lu, J.H.; Lee, C.H.; Chai, C.Y.; Yu, H.S. Anti-Inflammatory Effects Induced by Near-Infrared Light Irradiation through M2 Macrophage Polarization. *J Invest Dermatol* **2021**, *141*, 2056-2066 e2010, doi:10.1016/j.jid.2020.11.035.
15. Yang, Y.; Kim, O.S.; Liu, G.; Lee, B.N.; Liu, D.; Fu, W.; Zhu, S.; Kang, J.S.; Kim, B.; Kim, O. Effects of Red LED Irradiation in Enhancing the Mineralization of Human Dental Pulp Cells In Vitro. *Int J Mol Sci* **2023**, *24*, doi:10.3390/ijms24119767.
16. Fu, W.; Liu, G.; Kim, S.H.; Kim, B.; Kim, O.S.; Ma, G.; Yang, Y.; Liu, D.; Zhu, S.; Kang, J.S.; et al. Effects of 625 nm light-emitting diode irradiation on preventing ER stress-induced apoptosis via GSK-3beta phosphorylation in MC3T3-E1. *Photochem Photobiol* **2024**, doi:10.1111/php.13906.
17. Fu, W.I., Y.G.; Kim, B.; Kim, O.S.; Yang, Y.; Song, J.; Liu, D.; Zhu, S.; Kang, J.S.; Kim. O. 625 nm Light Irradiation Prevented MC3T3-E1 Cells from Accumulation of Misfolded Proteins via ROS and ATP Production. *Int. J. Mol. Sci.* **2023**, *24*, doi:10.3390/ijms24119257.
18. MF, D.E.O.; Johnson, D.S.; Demchak, T.; Tomazoni, S.S.; Leal-Junior, E.C. Low-intensity LASER and LED (photobiomodulation therapy) for pain control of the most common musculoskeletal conditions. *Eur J Phys Rehabil Med* **2022**, *58*, 282-289, doi:10.23736/s1973-9087.21.07236-1.
19. Sun, Q.; Kim, O.S.; He, Y.; Lim, W.; Ma, G.; Kim, B.; Kim, Y.; Kim, O. Role of E2F1/SPHK1 and HSP27 During Irradiation in a PMA-Induced Inflammatory Model. *Photobiomodul Photomed Laser Surg* **2020**, *38*, 512-520, doi:10.1089/photob.2019.4801.
20. do Valle, I.B.; Prazeres, P.; Mesquita, R.A.; Silva, T.A.; de Castro Oliveira, H.M.; Castro, P.R.; Freitas, I.D.P.; Oliveira, S.R.; Gomes, N.A.; de Oliveira, R.F.; et al. Photobiomodulation drives pericyte mobilization towards skin regeneration. *Sci Rep* **2020**, *10*, 19257, doi:10.1038/s41598-020-76243-7.
21. Zhu, G.; Zhang, T.; Chen, M.; Yao, K.; Huang, X.; Zhang, B.; Li, Y.; Liu, J.; Wang, Y.; Zhao, Z. Bone physiological microenvironment and healing mechanism: Basis for future bone-tissue engineering scaffolds. *Bioact Mater* **2021**, *6*, 4110-4140, doi:10.1016/j.bioactmat.2021.03.043.
22. Mosser, D.M.; Hamidzadeh, K.; Goncalves, R. Macrophages and the maintenance of homeostasis. *Cell Mol Immunol* **2021**, *18*, 579-587, doi:10.1038/s41423-020-00541-3.
23. Spiller, K.L.; Nassiri, S.; Witherel, C.E.; Anfang, R.R.; Ng, J.; Nakazawa, K.R.; Yu, T.; Vunjak-Novakovic, G. Sequential delivery of immunomodulatory cytokines to facilitate the M1-to-M2 transition of macrophages and enhance vascularization of bone scaffolds. *Biomaterials* **2015**, *37*, 194-207, doi:10.1016/j.biomaterials.2014.10.017.
24. Zhu, S.; Zhou, J.; Xie, Z. The balance between helper T 17 and regulatory T cells in osteoimmunology and relevant research progress on bone tissue engineering. *Immunity, Inflammation and Disease* **2024**, *12*, doi:10.1002/iid3.70011.
25. Han, S.; Chen, Z.; Han, P.; Hu, Q.; Xiao, Y. Activation of Macrophages by Lipopolysaccharide for Assessing the Immunomodulatory Property of Biomaterials<sup/>. *Tissue Eng Part A* **2017**, *23*, 1100-1109, doi:10.1089/ten.tea.2016.0501.
26. McWhorter, F.Y.; Wang, T.; Nguyen, P.; Chung, T.; Liu, W.F. Modulation of macrophage phenotype by cell shape. *Proc Natl Acad Sci U S A* **2013**, *110*, 17253-17258, doi:10.1073/pnas.1308887110.
27. Wu, H.; Yin, Y.; Hu, X.; Peng, C.; Liu, Y.; Li, Q.; Huang, W.; Huang, Q. Effects of Environmental pH on Macrophage Polarization and Osteoimmunomodulation. *ACS Biomater Sci Eng* **2019**, *5*, 5548-5557, doi:10.1021/acsbiomaterials.9b01181.

28. Olson, H.M.; Nechiporuk, A.V. Lamellipodia-like protrusions and focal adhesions contribute to collective cell migration in zebrafish. *Dev Biol* **2021**, *469*, 125-134, doi:10.1016/j.ydbio.2020.10.007.
29. Mylvaganam, S.; Freeman, S.A.; Grinstein, S. The cytoskeleton in phagocytosis and macropinocytosis. *Curr Biol* **2021**, *31*, R619-r632, doi:10.1016/j.cub.2021.01.036.
30. Cougoule, C.; Van Goethem, E.; Le Cabec, V.; Lafouresse, F.; Dupré, L.; Mehraj, V.; Mège, J.L.; Lastrucci, C.; Maridonneau-Parini, I. Blood leukocytes and macrophages of various phenotypes have distinct abilities to form podosomes and to migrate in 3D environments. *Eur J Cell Biol* **2012**, *91*, 938-949, doi:10.1016/j.ejcb.2012.07.002.
31. Hind, L.E.; Lurier, E.B.; Dembo, M.; Spiller, K.L.; Hammer, D.A. Effect of M1-M2 Polarization on the Motility and Traction Stresses of Primary Human Macrophages. *Cell Mol Bioeng* **2016**, *9*, 455-465, doi:10.1007/s12195-016-0435-x.
32. Fan, S.; Sun, X.; Su, C.; Xue, Y.; Song, X.; Deng, R. Macrophages-bone marrow mesenchymal stem cells crosstalk in bone healing. *Front Cell Dev Biol* **2023**, *11*, 1193765, doi:10.3389/fcell.2023.1193765.
33. Shojaee, P.; Mornata, F.; Deutsch, A.; Locati, M.; Hatzikirou, H. The impact of tumor associated macrophages on tumor biology under the lens of mathematical modelling: A review. *Front Immunol* **2022**, *13*, 1050067, doi:10.3389/fimmu.2022.1050067.
34. Ding, H.; Zhang, Y.; Mao, Y.; Li, Y.; Shen, Y.; Sheng, J.; Gu, N. Modulation of macrophage polarization by iron-based nanoparticles. *Med Rev (2021)* **2023**, *3*, 105-122, doi:10.1515/mr-2023-0002.
35. Chen, X.; Wan, Z.; Yang, L.; Song, S.; Fu, Z.; Tang, K.; Chen, L.; Song, Y. Exosomes derived from reparative M2-like macrophages prevent bone loss in murine periodontitis models via IL-10 mRNA. *J Nanobiotechnology* **2022**, *20*, 110, doi:10.1186/s12951-022-01314-y.
36. Tylek, T.; Blum, C.; Hrynevich, A.; Schlegelmilch, K.; Schilling, T.; Dalton, P.D.; Groll, J. Precisely defined fiber scaffolds with 40 mum porosity induce elongation driven M2-like polarization of human macrophages. *Biofabrication* **2020**, *12*, 025007, doi:10.1088/1758-5090/ab5f4e.
37. Safadi, F.F.; Barbe, M.F.; Abdelmagid, S.M.; Rico, M.C.; Aswad, R.A.; Litvin, J.; Popoff, S.N. Bone Structure, Development and Bone Biology. In *Bone Pathology*, 2009; pp. 1-50.
38. Komori, T. Regulation of osteoblast differentiation by Runx2. *Adv Exp Med Biol* **2010**, *658*, 43-49, doi:10.1007/978-1-4419-1050-9_5.
39. Zainal Ariffin, S.H.; Lim, K.W.; Megat Abdul Wahab, R.; Zainal Ariffin, Z.; Rus Din, R.D.; Shahidan, M.A.; Johari, A.N.; Zainol Abidin, I.Z. Gene expression profiles for in vitro human stem cell differentiation into osteoblasts and osteoclasts: a systematic review. *PeerJ* **2022**, *10*, e14174, doi:10.7717/peerj.14174.
40. Zhu, S.; Chen, W.; Masson, A.; Li, Y.P. Cell signaling and transcriptional regulation of osteoblast lineage commitment, differentiation, bone formation, and homeostasis. *Cell Discov* **2024**, *10*, 71, doi:10.1038/s41421-024-00689-6.
41. Zhou, P.; Shi, J.M.; Song, J.E.; Han, Y.; Li, H.J.; Song, Y.M.; Feng, F.; Wang, J.L.; Zhang, R.; Lan, F. Establishing a deeper understanding of the osteogenic differentiation of monolayer cultured human pluripotent stem cells using novel and detailed analyses. *Stem Cell Res Ther* **2021**, *12*, 41, doi:10.1186/s13287-020-02085-9.
42. Suh, K.; Cho, Y.K.; Breinyn, I.B.; Cohen, D.J. E-cadherin biomaterials reprogram collective cell migration and cell cycling by forcing homeostatic conditions. *Cell Rep* **2024**, *43*, 113743, doi:10.1016/j.celrep.2024.113743.
43. dos Santos, G.; Rogel, M.R.; Baker, M.A.; Troken, J.R.; Urich, D.; Morales-Nebreda, L.; Sennello, J.A.; Kutuzov, M.A.; Sitikov, A.; Davis, J.M.; et al.

Vimentin regulates activation of the NLRP3 inflammasome. *Nat Commun* **2015**, *6*, 6574, doi:10.1038/ncomms7574.
44. Cheng, F.; Shen, Y.; Mohanasundaram, P.; Lindstrom, M.; Ivaska, J.; Ny, T.; Eriksson, J.E. Vimentin coordinates fibroblast proliferation and keratinocyte differentiation in wound healing via TGF-beta-Slug signaling. *Proc Natl Acad Sci U S A* **2016**, *113*, E4320-4327, doi:10.1073/pnas.1519197113.
45. Ostrowska-Podhorodecka, Z.; Ding, I.; Norouzi, M.; McCulloch, C.A. Impact of Vimentin on Regulation of Cell Signaling and Matrix Remodeling. *Front Cell Dev Biol* **2022**, *10*, 869069, doi:10.3389/fcell.2022.869069.
46. Huang, X.; Zhu, L.; Gong, Y. Rhein induces bone regeneration via alleviating inflammation in murine periodontitis model. *Oral Dis* **2024**, *30*, 1506-1515, doi:10.1111/odi.14502.
47. Zhu, D.; Yu, H.; Liu, P.; Yang, Q.; Chen, Y.; Luo, P.; Zhang, C.; Gao, Y. Calycosin modulates inflammation via suppressing TLR4/NF-κB pathway and promotes bone formation to ameliorate glucocorticoid-induced osteonecrosis of the femoral head in rat. *Phytother Res* **2021**, *35*, 2824-2835, doi:10.1002/ptr.7028.
48. Osta, B.; Benedetti, G.; Miossec, P. Classical and Paradoxical Effects of TNF-α on Bone Homeostasis. *Front Immunol* **2014**, *5*, 48, doi:10.3389/fimmu.2014.00048.
49. Zhang, F.; Lv, M.; Wang, S.; Li, M.; Wang, Y.; Hu, C.; Hu, W.; Wang, X.; Wang, X.; Liu, Z.; et al. Ultrasound-triggered biomimetic ultrashort peptide nanofiber hydrogels promote bone regeneration by modulating macrophage and the osteogenic immune microenvironment. *Bioact Mater* **2024**, *31*, 231-246, doi:10.1016/j.bioactmat.2023.08.008.
50. Chen, Z.; Klein, T.; Murray, R.Z.; Crawford, R.; Chang, J.; Wu, C.; Xiao, Y. Osteoimmunomodulation for the development of advanced bone biomaterials. *Materials Today* **2016**, *19*, 304-321, doi:10.1016/j.mattod.2015.11.004.
51. Liu, T.; Li, F.; Yan, Y.; Gao, S.; Zhou, D.; Jiang, X.; Song, C.; Fu, Z.; Liu, Z. The Role of Persistent Inflammation in the Pathogenesis of Infected Nonunion: A Narrative Review. *Immun Inflamm Dis* **2025**, *13,* e70260, doi:10.1002/iid3.70260.

Supplementary Files

This is a list of supplementary files associated with this preprint. Click to download.

- SupplementaryData.pdf